Nonlinear Effects in LTE Downlink Signals and Application of a Compensation Technique at the Receiver Side

Michel Allegue-Martínez, María J. Madero-Ayora, Carlos Crespo-Cadenas, Javier Reina-Tosina and Francisco Bernardo

Dpto. de Teoría de la Señal y Comunicaciones

Escuela Superior de Ingenieros, Universidad de Sevilla

Camino de los Descubrimientos, s/n.; 41092 -- Seville, Spain

Phone: +34 95 4487334; Fax: +34 95 4487341; E-mail: micallmar@alum.us.es

ABSTRACT

This paper proposes a nonlinear compensation technique for LTE downlink signals based on the memoryless solid-state power amplifier (SSPA) model which provides a simple and effective linearization technique in the receiver side, allowing a reduction in the error vector magnitude (EVM) measured characteristics. The EVM per subcarrier is analyzed for different appropriate resource blocks allocations in the LTE signal in order to examine the distortion due to the nonlinear effects produced by a power amplifier in the experimental setup.

INDEX TERMS

Memoryless compensator, LTE downlink signal, nonlinear distortion, power amplifier.

I. INTRODUCTION

The advent of Long Term Evolution (LTE) technologies is expected to fuel a vast development of next-generation services and applications. The LTE standard implements the Orthogonal Frequency Division Multiplexing (OFDM) as the modulation technique. This modulation has been proved to be sensitive to impairments such as IQ imbalance, phase noise and nonlinearities [1]. The high peak-to-average power ratio (PAPR) exhibited by OFDM signals makes nonlinear distortion a major system impairment [2].

Important progress has been made in the predistortion techniques to linearize the power amplifier output, implying a more efficient usage of this device [3]. However, due to the spectral mask emission itself, defined in all mobile communications standards, a residual spectral regrowth is allowed in the transmitter. In addition to this, other components of the communications system could introduce nonlinear behaviors, such as the own receiver. Because of this, a receiver-based compensation technique could be used to linearize the output of the communication system [4]. This technique can coexist with the predistortion mechanisms as a complement to increase the robustness of the system.

In this paper, we propose a compensation technique to mitigate the nonlinear distortion effects in the receiver, produced by a power amplifier on LTE signals, and a study of the error vector magnitude (EVM) behavior for different resource allocations. The compensation technique is applied to measured signals and the EVM is analyzed from an experimental point of view. The paper is organized as follows: in Section II an overview of the LTE physical layer characteristics will be given, in Section III the compensation mechanism is obtained based on a simple nonlinear model; Section IV contains experimental results and discussion about the EVM degradation of the considered LTE signals across a nonlinearity and finally, some conclusions will be presented.

II. OVERVIEW OF THE CONSIDERED LTE SIGNALS

The considered signals for the experimental study of this paper follow the LTE-downlink standard with a subcarrier separation of 15 kHz to implement the ODFM. The transmitted signal in each slot of 0.5 ms duration is described by a resource grid in the frequency and time domains. The mapping of physical channels is made in terms of Physical Resource Blocks (PRBs), each including 12 adjacent subcarriers in the frequency domain and 7 consecutive OFDM symbols in the time domain. For the normal cyclic prefix (CP) configuration, the first symbol in each slot uses a different CP length from the rest [5].

A channel bandwidth of 5 MHz has been chosen, for which there are 25 PRBs available, i.e. 300 useful subcarriers [6]. The center subcarrier of the channel corresponds to dc in baseband and thus is not transmitted in the downlink. The Single Input Single Output (SISO) system described in Fig. 1 was used to create and test the LTE signals. The baseband 16-QAM input symbols are assigned to the 300 available subcarriers on each OFDM symbol through a serial-to-parallel converter. Then, these parallel-allocated symbols go into an IFFT (Inverse Fast Fourier Transform) block with $N = 2048$ points and are parallel-to-serial converted into a vector that contains the time domain samples. The CP is added before the signal is up-converted to the RF carrier frequency (f_c) using a transmitter (Tx) front-end in the experimental setup. The inverse operations, beginning with the CP removal (RCP) process, were performed at the receiver (Rx) side. An experimental setup, with a power amplifier (PA) as the principal source of nonlinearities, was placed between the OFDM modulator and demodulator to validate the nonlinear compensator effectiveness. The experimental setup will be described in Section IV.

Depending on the kind of transmitted physical channel and the traffic to allocate, a different number of PRBs will be active out of the 25 available. Each of these PRBs will be denoted by a number meaning its position, n_{PRB}. In this work, we chose to study certain configurations for the active PRBs as shown in Fig. 2, considering that the expected nonlinear effects may lead to different performances depending on the signal. For example, we expect a different impact of distortion when only the smallest possible bandwidth is occupied with

respect to the case in which all the available bandwidth is used. More differences are likely depending on the frequency shift of the active resource blocks with respect to the center frequency. Fig. 2 depicts the four adopted PRB allocations. In type A signals, only one PRB is active and its position is changed along the possible allocations, being the cases under study those for n_{PRB} = 1, 4, 7, 10 and 13. Type B signals present two active PRBs occupying alternative positions, being the cases under study given by the pairs n_{PRB} = {1, 3}; {6, 8}; and {12, 14}. In signal C, alternate PRBs are active occupying the whole bandwidth, which corresponds to the odd values of n_{PRB}. Finally, signal D represents the case in which all the PRBs are active.

III. IMPLEMENTATION OF THE MEMORYLESS NONLINEAR COMPENSATION TECHNIQUE

In order to get a better power efficiency, the PAs in the base stations might be operated near the saturation region, producing non-negligible nonlinear distortion. The major sources of nonlinearity are the analogue-to-digital and digital-to-analogue converters, mixers and amplifiers, i.e. the PA in the Tx and the low-noise amplifier in the Rx [7]. In this paper, a memoryless nonlinear compensator is proposed to be implemented as the first baseband block in the receiver side.

Denoting the complex envelope input to the PA as $\tilde{x}(t)$ and the complex envelope output as $\tilde{y}(t)$, the solid-state PA model prediction of the static amplitude-to-amplitude modulation (AM/AM) characteristic could be written in the form:

$$\left|\tilde{y}(t)\right| = \frac{G_0 \left|\tilde{x}(t)\right|}{\left[1+\left(\frac{G_0 \left|\tilde{x}(t)\right|}{A_0}\right)^{2p}\right]^{\frac{1}{2p}}}, \tag{1}$$

where G_0 represents the small-signal gain in the system, A_0 is the maximum output amplitude

and the parameter p controls the smoothness of the transition between the linear and saturated regions. The parameter α_ϕ controls the strength of the phase distortion in the amplitude-to-phase modulation (AM/PM) characteristic [8]:

$$\phi(t) = \alpha_\phi \left(\frac{G_0 |\tilde{x}(t)|}{A_0} \right)^4 . \tag{2}$$

The simplicity of this model allows a compensation technique with only four coefficients. This technique basically consists on the cancellation of the denominator in (1) by using the received samples of the signal and the coefficients that better describe the nonlinear behavior along the whole communication system. With the previously estimated coefficients we can obtain the inverse of the nonlinearity by means of a closed-form expression and apply the compensation in the Rx to mitigate the distortion effects. The linearized output complex envelope of the compensator, denoted by $\tilde{y}_{lin}(t)$, can be computed from the AM/AM and AM/PM characteristics (3) and (4), respectively.

$$|\tilde{y}_{\text{lin}}(t)| = |\tilde{x}(t)| = \frac{|\tilde{y}(t)|}{G_0} \left[1 - \left(\frac{|\tilde{y}(t)|}{A_0} \right) \right]^{-\frac{1}{2p}} \tag{3}$$

$$\phi_{\text{lin}}(t) = -\alpha_\phi \left[\left(\frac{A_0}{|\tilde{y}(t)|} \right)^{2p} - 1 \right]^{-\frac{2}{p}} \tag{4}$$

The three first OFDM symbols of each measured signal have been employed as a training sequence to identify the coefficients of the inverse model. With these coefficients on (3), the compensator is fully configured to mitigate the nonlinear distortion effects of the entire signal at the Rx side. Despite its simplicity, it will be shown in Section IV that a satisfactory reduction of the EVM in the received signals can be achieved by the application of this technique.

IV. EXPERIMENTAL RESULTS AND DISCUSSION

The experimental setup used for the measurements of this study is detailed in Fig.1. After the OFDM modulation process performed by software in the Tx side, the different LTE signals were loaded into a Rohde & Schwarz vector signal modulator SMIQ02B with built-in arbitrary waveform facility. For the signal acquisition process an Agilent EXA N9010A vector analyzer was employed, equipped with the VSA software. A medium-high PA (model ZHL42W of MiniCircuits Inc., Brooklyn, NY) exhibiting a gain over 30 dB in the frequency range 10-4200 MHz, with a minimum output 1-dB compression point (P_{1dB}) of +28 dBm was used as the principal nonlinear source in the communication channel. A center frequency of 2 GHz has been selected for the signal generator and an input level sweep was performed from -16 dBm to -6 dBm, around the PA P_{1dB}.

When all the signals were correctly acquired in the receiver for different input levels and OFDM demodulated, two definitions of EVM have been used to evaluate the dispersion of the received 16-QAM symbols around their ideal constellation point due to the nonlinearities present in the communication system. The first one is the widely employed root mean square EVM computed by:

$$\mathrm{EVM} = \sqrt{\frac{\sum |\tilde{y} - \tilde{y}_{\mathrm{ref}}|^2}{\sum |\tilde{y}_{\mathrm{ref}}|^2}}. \tag{5}$$

where, $\tilde{y}_{\mathrm{ref}}$ is the reference signal and $\tilde{y}$ the signal whose dispersion needs to be quantized. Furthermore, it is interesting to study more in detail the in-band interference. The second figure of merit is used to compute the error vector magnitude on each subcarrier and, in order to include the subcarriers that contain zeros, a new normalization in (5) is necessary using the outermost symbol magnitude that will be denoted as EVM_{osmn} [9].

EVM values were not measured directly from the EXA vector analyzer or VSA software because the demodulator block does not know the transmitted data and the acquired signal is strongly affected by the nonlinear effects, making difficult to deduce the correct

reference. In these cases, it is recommendable to compute the EVM with knowledge of the reference symbols.

To analyze the nonlinear effects over the LTE signal, let us consider the type A signals in Fig. 2 for different input levels, even though all the previously defined types of signals have been used to analyze the in-band interference. Once the OFDM demodulation has been carried out, the EVM_{osmn} over each subcarrier was computed for the cases $n_{PRB} = 1,\ 7,\ 13$ and simultaneously represented in Fig. 3 for three different input levels on each case of study. In this figure and Fig. 5, the vertical lines are delimiting the 25 PRBs, allocated from subcarrier number 107 to subcarrier 407. When the output level is nearer the output saturation point of the PA an important increase of the EVM_{osmn} is detected in the active PRBs and in the adjacent subcarriers. This interference vanishes while the input level goes down, although there is a persistent degradation of the EVM_{osmn} due to the interference of the twelve actives subcarriers over the subcarriers set to "0" at the left and right sides of the active PRB. These effects are mitigated with the use of an inefficient input level of -13 dBm, as illustrated in Fig. 3 for the three cases of signals type A. The same observations were done for $n_{PRB} = 4$ and 10.

For an efficient usage of the PA features and a good system response with respect to nonlinearities, keeping the errors below the LTE requirements, the memoryless nonlinear compensation technique was applied for all the signals under study and its results are represented in Fig. 4. In this case, the root mean square EVM is presented. As it was expected, markers in Fig. 4 show an increase of the measured values of EVM (%) as the input signal level approaches the PA P_{1dB} for all the signals under study. Slight differences can be observed between the behaviors of each EVM characteristic for the employed signals. However, types A and B signals exhibited identical behaviors between each allocation for the same signal, and we have plotted one of these cases; only for type A signal with $n_{PRB} = 13$, i.e. the center PRB, smaller values of EVM were measured for input levels of -7 dBm and -6 dBm.

As it is illustrated by Fig. 4, the input levels above -8 dBm cannot be used in an LTE environment because the measured EVM is greater than the 12.5% allowed in the standard, due to the nonlinear distortion. However, the implementation of the nonlinear compensation detailed in Section III makes possible the utilization of these operation points, resulting in a more efficient employment of the PA.

Despite the use of a static nonlinear model with only four coefficients, the predicted EVM values are adequate enough; even though the prediction for the highest input levels are a little below the measured ones, possibly due to the intensification of the memory effects for this operation region. However, the adopted model represents the general behavior of the measured characteristics and allows the nonlinear compensation at the Rx side as demonstrated in Fig. 4. The compensated measurements exhibit improved EVM characteristics for all the generated signals, obtaining EVM reductions up to 5.6% for a more usual situation in an LTE environment, as signal D is.

In Fig. 5, it has been represented simultaneously the EVM_{osmn} per each subcarrier for type B signals in the cases $n_{PRB} = \{1, 3\}$ and $\{12, 14\}$, when an input level of -8 dBm has been selected. This figure reveals an increase of EVM_{osmn} on inactive PRBs adjacent to the active ones, especially at PRB number 5 and its image respect to the center frequency for the case $n_{PRB} = \{1, 3\}$. The same happens for PRBs number 10 and 16 due to the transmission over $n_{PRB} = \{12, 14\}$ and for type B signal with $n_{PRB} = \{4, 6\}$ that is not shown in the figure. A similar behavior was discussed in Fig. 3 for type A signals. Once again, the compensation mechanism obtains EVM_{osmn} differences up to 3.5% between the non-compensated and compensated measurements per each subcarrier.

For signals C and D the EVM_{osmn} of the unused subcarriers is incremented by the adjacent active subcarriers that contain 16-QAM symbols. When all PRBs are allocated as in signal D, the EVM_{osmn} is higher than in the other cases. To analyze more in details the proposed memoryless compensation technique, the measurement signals type C and D were

tested after the acquisition process into an additive white Gaussian noise (AWGN) channel simulation. The measurements for the -8 dBm input level were selected to analyze the bit error rate (BER) versus the signal to noise ratio (SNR).

Fig. 6 shows that signals C and D were highly distorted with respect to the linear cases due to the PA nonlinearities. The input level of these signals is 3 dB below the 1 dB input compression point and the degradation observed in the system performance is not acceptable in an LTE environment. However, the compensation technique allows the use of this input level, getting a BER of 10^{-6} for reasonable SNR values on types C and D signals, with an efficient usage of the PA. The SNR gain for a 1.43×10^{-4} BER value is above 8 dB for signal D, while for the case of signal C the SNR gain is over 9 dB to keep a BER of 2.21×10^{-5}. The EVM_{osmn} of these two signals was analyzed and it can be checked that the compensation technique reduces this figure in a similar way to the case of two active PRBs shown in Fig. 5.

CONCLUSIONS

This paper discusses the nonlinear effects on LTE-downlink signals from an experimental point of view. The intercarrier interference has been analyzed with the EVM_{osmn} per subcarrier for different PRB allocations and it has been shown that there is an EVM increase produced by the active PRBs over their adjacent PRBs, active or not. A memoryless nonlinear compensation technique has been applied to linearize the distorted signals in the receiver side with good results. Input levels not allowed in the standard due to the regrowth of EVM values are possible with this technique, employing the PA efficiently and with the low computational cost of a four coefficients nonlinear compensator.

ACKNOWLEDGMENTS

This work was supported by the Spanish National Board of Scientific and Technological Research (CICYT) under Project TEC2008-06259/TEC, and by the Regional Government of Andalusia (CICE) under Grant P07-TIC-02649. The work of Mr. Allegue was

supported by the Spanish Ministry of Foreign Affairs and Cooperation and the Spanish Agency of International Cooperation for Development.

REFERENCES

[1] C. Galiotto, Y. Huang, N. Marchetti, and M. Zorzi, Performance Evaluation of Non-Ideal RF Transmitter in LTE/LTE-Advanced Systems, in IEEE European Wireless Conference Proceedings, Aalborg, Denmark, Oct. 2009, pp. 266-270.

[2] A. Chorti and M. Brookes, On the Effects of Memoryless Nonlinearities on M-QAM and DQPSK OFDM Signals, IEEE Transactions on Microwave Theory and Techniques, 54 (8), pp.3301-3315, Aug. 2006.

[3] A. Zhu, P.J Draxler, J.J. Yan, T.J. Brazil, D.F. Kimball and P.M. Asbeck, Open-Loop Digital Predistorter for RF Power Amplifiers Using Dynamic Deviation Reduction-Based Volterra Series, IEEE Transactions on Microwave Theory and Techniques, 56 (7), pp.1524-1534, Jul. 2008.

[4] C. Dehos and T. C. W. Schenk, Digital Compensation of Amplifier Nonlinearities in the Receiver of a Wireless System, in IEEE 14th Symposium on Communication and Vehicular Technology in the Benelux, Delft, The Netherlands, Nov. 2007, pp. 1-6.

[5] 3GPP TS 36.211 v8.9.0 Release 8, LTE; Evolved Universal Terrestrial Radio Access (E-UTRA); Physical Channels and Modulation, Jan. 2010.

[6] 3GPP TS 36.104 v8.10.0 Release 8, LTE; Evolved Universal Terrestrial Radio Access (E-UTRA); Base Station (BS) Radio Transmission and Reception, Jul. 2010.

[7] T. Schenk, RF Imperfections in High-rate Wireless Systems. Impact and Digital Compensation, Springer, 2008.

[8] E. Costa and S. Pupolin, M-QAM-OFDM System Performance in the Presence of a Nonlinear Amplifier and Phase Noise, IEEE Transactions on Communications, 50 (3), pp. 462-472, Mar. 2002.

[9] Agilent AN 1314, Testing and Troubleshooting Digital RF Communications Receiver Designs, Agilent Technologies Application Note.

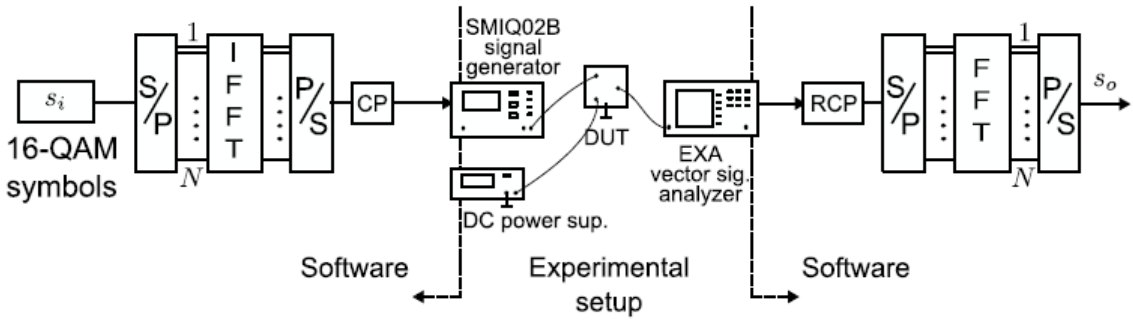

Figure 1. Block diagram for the implemented LTE downlink system and the experimental setup.

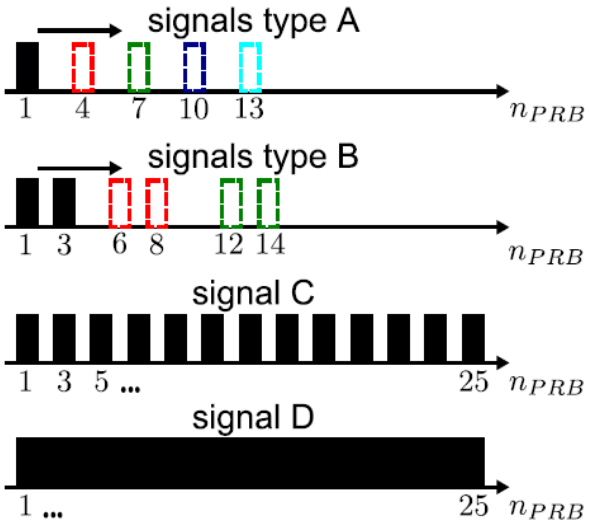

Figure 2. Diagram of the considered signals with different PRB allocations.

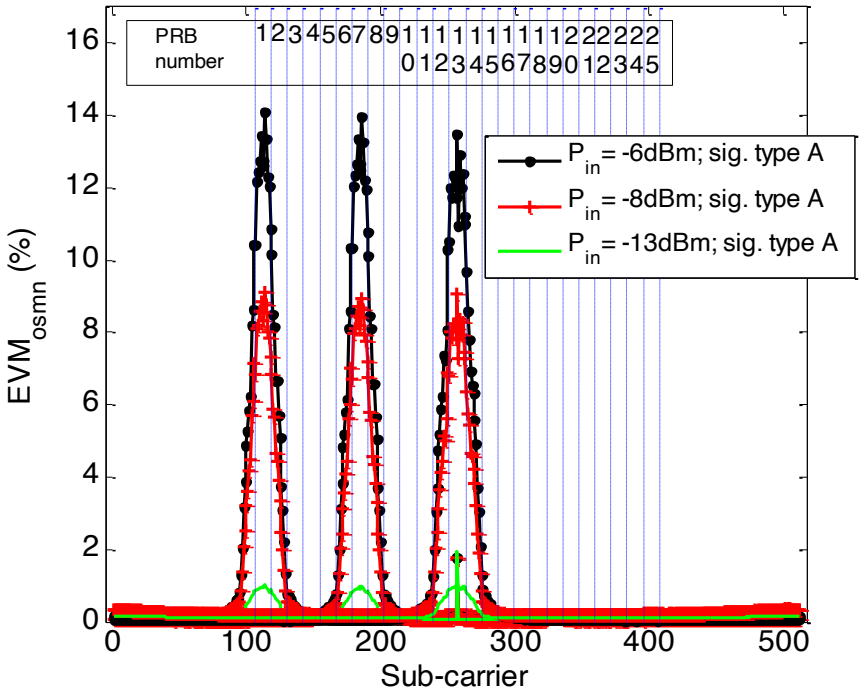

Figure 3. Simultaneous representations of the EVM_{osmn} per subcarrier for measured type A signals for the cases n_{PRB} = 1, 7 and 13 (only one active PRB) and input levels of -6dB$_m$ (black line), -8dB$_m$ (red dashed line) and -13dB$_m$ (green line).

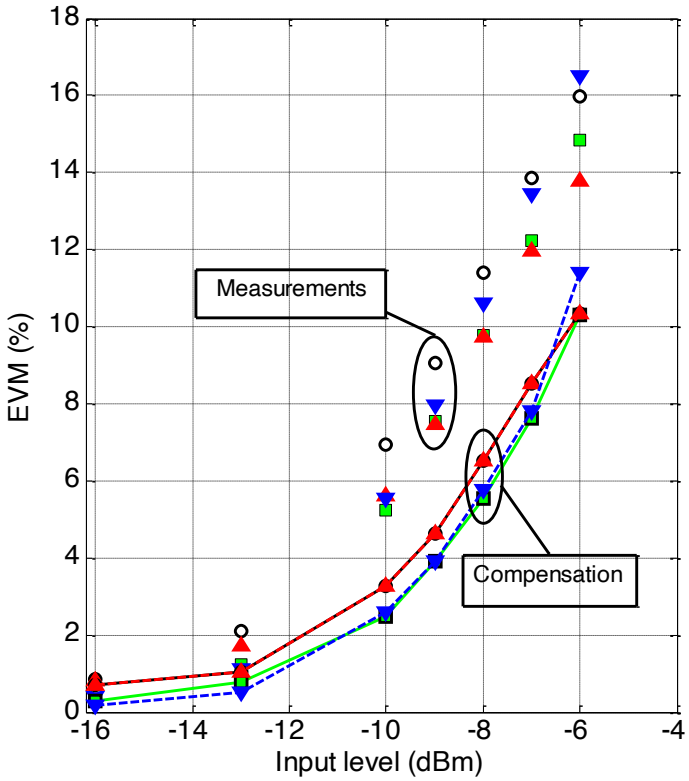

Figure 4. EVM of measured and compensated signals for the cases considered in Fig. 2. Markers only represent the measurements of the different signal types in correspondence with: downward blue triangles, A; green squares, B; upward red triangles, C and white circles; D. Lines (dashed blue, A; solid green, B; dashed red, C; solid black, D) and markers in concordance with previous styles represent the EVM obtained after the nonlinear compensation.

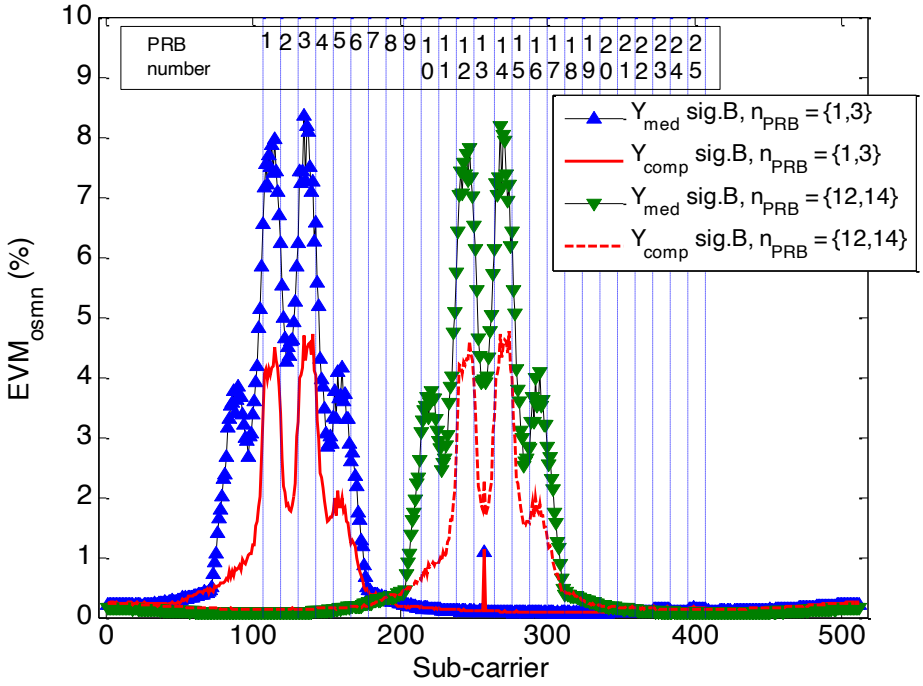

Figure 5. Simultaneous representation of the EVM_{osmn} per subcarrier for measured (Ymed) and compensated (Ycom) type B signals for the cases n_{PRB} = {1, 3} and {12, 14} for an input level of -8 dBm.

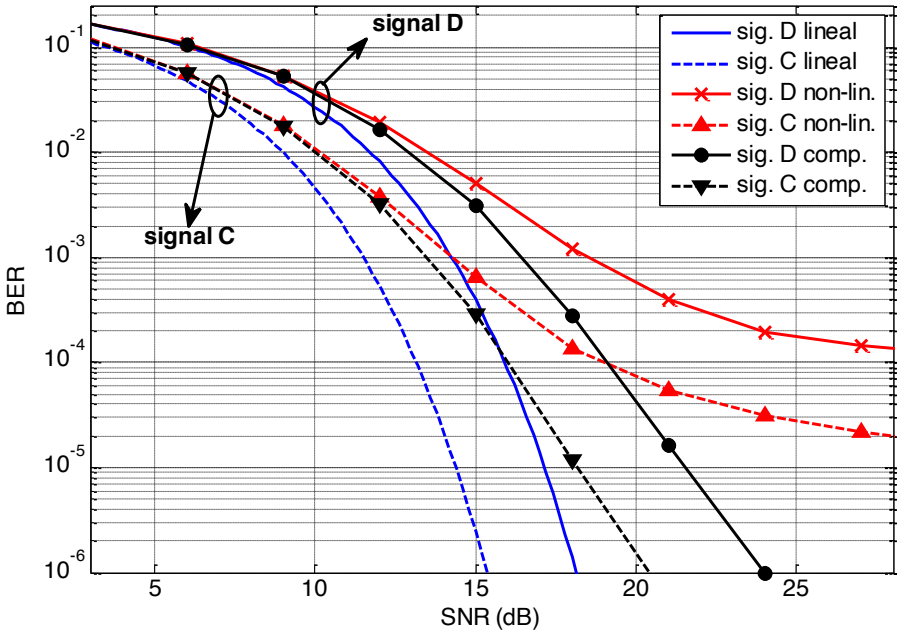

Figure 6. BER versus SNR curves for types C and D signals. For each of them it has been computed the linear case, the distorted signal and the compensated one at the receiver side with the technique proposed in this paper.